Downloaded from orbit.dtu.dk on: May 01, 2024

DTU Library

Scalable and highly tunable conductive oxide interfaces

Cohen-Azarzar, Dana; Baskin, Maria; Lindblad, Andreas; Trier, Felix; Kornblum, Lior

Published in:
APL Materials

Link to article, DOI:
10.1063/5.0174283

Publication date:
2023

Document Version
Publisher's PDF, also known as Version of record

Link back to DTU Orbit

Citation (APA):
Cohen-Azarzar, D., Baskin, M., Lindblad, A., Trier, F., & Kornblum, L. (2023). Scalable and highly tunable conductive oxide interfaces. *APL Materials*, *11*(11), Article 111118. https://doi.org/10.1063/5.0174283

General rights
Copyright and moral rights for the publications made accessible in the public portal are retained by the authors and/or other copyright owners and it is a condition of accessing publications that users recognise and abide by the legal requirements associated with these rights.

- Users may download and print one copy of any publication from the public portal for the purpose of private study or research.
- You may not further distribute the material or use it for any profit-making activity or commercial gain
- You may freely distribute the URL identifying the publication in the public portal

If you believe that this document breaches copyright please contact us providing details, and we will remove access to the work immediately and investigate your claim.

Scalable and highly tunable conductive oxide interfaces

Cite as: APL Mater. 11, 111118 (2023); doi: 10.1063/5.0174283
Submitted: 29 August 2023 • Accepted: 27 October 2023 •
Published Online: 17 November 2023

View Online

Export Citation

CrossMark

Dana Cohen-Azarzar,[1] Maria Baskin,[1] Andreas Lindblad,[2] Felix Trier,[3] and Lior Kornblum[1,a)]

AFFILIATIONS

[1] The Andrew and Erna Viterbi Department of Electrical and Computer Engineering, Technion–Israel Institute of Technology, Haifa 32000-03, Israel
[2] Department of Physics and Astronomy, Uppsala University, 752 36 Uppsala, Sweden
[3] Department of Energy Conversion and Storage, Technical University of Denmark, 2800 Kgs. Lyngby, Denmark

[a)] Author to whom correspondence should be addressed: liork@technion.ac.il

ABSTRACT

Conducting oxide interfaces have attracted considerable attention, motivated by both fundamental science and potential for oxide electronic devices. An important gap for maturing such device technology is scalability and routes to control the electronic properties, which can narrow the device engineering space. Here, we demonstrate and explain the mechanisms of highly tunable conductive oxide interfaces. We synthesized amorphous–crystalline $Al_2O_3/SrTiO_3$ interfaces using the scalable and industry-compatible atomic layer deposition (ALD) technique. An NH_3 plasma pretreatment is employed in the ALD chamber, and its duration is used as a tuning parameter for the electrical properties, where a span of three orders of magnitude in the sheet resistance is observed at room temperature. For the most conductive sample, our results are comparable to the highest carrier density values reported for all-crystalline oxide interfaces prepared with state-of-the-art epitaxial growth techniques, such as pulsed laser deposition. We pinpoint the origin of conductivity to oxygen vacancies caused by the $SrTiO_3$ reduction by the NH_3 plasma pretreatment. These results present a simple, scalable, and industry-compatible route for realizing conductive oxide interfaces, with a broad parameter space, offering a versatile and flexible toolkit for oxide device engineering.

© 2023 Author(s). All article content, except where otherwise noted, is licensed under a Creative Commons Attribution (CC BY) license (http://creativecommons.org/licenses/by/4.0/). https://doi.org/10.1063/5.0174283

06 December 2023 08:50:58

I. INTRODUCTION

Emergent conductivity at oxide interfaces[1] has attracted considerable interest over the past two decades, owing to its rich physics and potential for device applications. This phenomenon is commonly termed a (quasi) 2D electron gas (2DEG), referring to its interfacial nature. The mechanisms behind the formation of oxide 2DEGs at the interface have been attributed to polar discontinuity[2] and ionic defects. The latter mechanism is commonly attributed to oxygen vacancies,[1,3–5] while doping caused by interface intermixing[6,7] and other defects[8] have also been shown to play a role. Some recent descriptions combine these pictures, invoking interactions between polarity and defects as the mechanism for conductivity.[9–11] We note that for the sake of simplicity, we broadly and loosely use the term "2DEGs" to describe conductive oxide interfaces, whereas *quasi*-2D or other terms might be more accurate.

While research into the fundamentals of oxide 2DEGs persists, there is a growing interest in harnessing this phenomenon toward useful devices. Oxide 2DEGs have been gaining traction for their potential as channels in field effect transistors,[12–15] gas sensors,[16,17] spintronic devices,[18–20] and resistive random access memories (ReRAMs).[21–25] Maturation of these device applications and the development of new devices require the ability to deterministically control the electrical properties of 2DEGs and to synthesize them in an industrially compatible process. These crucial abilities are needed for enabling such devices, and engineering their properties, such as the on–off ratio and subthreshold slope of field effect transistors, sensitivity of chemical sensors, mitigation of parasitic effects, and other important performance parameters.

Oxide 2DEGs have been most commonly studied at the $LaAlO_3/SrTiO_3$ (LAO/STO) interface,[1] where the former is epitaxially grown on a single crystal substrate of the latter. This material

system is typically synthesized by pulsed laser deposition (PLD), which can provide excellent crystalline quality and atomic-scale precision. While these features are particularly useful for scientific purposes, PLD has limits for technological applications owing to its low throughput compared to microelectronics-compatible processes and significant costs in operating PLD systems (e.g., procuring excimer laser gas), which limits the scalability and prospects of mass production. To overcome this hurdle, 2DEGs were realized using atomic layer deposition (ALD) of various oxides on STO substrates,[26–28] followed by an "all-ALD" approach that circumvents the need for STO substrates.[14,29] ALD is a highly scalable and versatile process,[30,31] and it is an integral part of any modern microelectronics fabrication flow. As such, ALD provides a route for synthesizing highly scalable and microelectronics-compatible 2DEGs that can push oxide electronics closer to practical realization. However, this approach can suffer from low charge carrier densities in the resulting oxide 2DEGs (leading to high resistances), which are not easily tunable.

Here, we demonstrate and illustrate the mechanisms of a new approach for 2DEG formation with ALD, providing a broad tunability of the electronic properties. This approach is based on an *in situ* pretreatment in the ALD chamber, allowing for three orders of magnitude tunability in the conductivity via the carrier density at room temperature (and at least six orders at 50 K). This method preserves the structure of the interface and the smoothness of the free surface—critical features for oxide electronic devices, such as memristors and transistors. The mechanism of this tunability is pinpointed to a controlled reduction of the substrate surface during pretreatment, where its duration provides a simple and robust tuning parameter.

II. EXPERIMENTAL

Undoped (001) STO substrates ($5 \times 5 \times 0.5$ mm^3, CrysTec GmbH) were TiO_2-terminated with the HF method.[32] These substrates were heated to 300 °C and subjected to a NH_3 plasma treatment performed in the ALD chamber, which induced conductivity at the STO surface by reduction. The NH_3 plasma exposure (~40 mTorr, 300 W) was performed in cycles of 30 s each, and the total time was varied between 0 and 4 min. To avoid reoxidation of the STO surface following atmospheric exposure, all samples were capped with a nominally 4 nm amorphous Al_2O_3 layer, grown by atomic layer deposition (ALD, Ultratech/Cambridge Nanotech Fiji G2). The Al_2O_3 growth was performed using trimethylaluminum (TMA) and water as the precursors[33] (0.1 s of TMA pulse, 10 s of purge, 0.3 s of water pulse, and 5 s of purge), keeping the substrate temperature at 300 °C. During the initial temperature ramping, the chamber pressure is ~15 mTorr (with several short Ar purges reaching a peak of ~7 Torr at a cycle of 3 min). The Al_2O_3 layer thickness is found to agree with the nominal values using x-ray reflectivity. Each plasma exposure and subsequent Al_2O_3 deposition were performed on two batches of substrates. The first batch includes four substrates simultaneously, where one representative sample from each process was selected for full analysis. See the full dataset (Table S1 and Fig. S2), details, and discussion of the effect of light exposure in the supplementary material. The second batch included only one sample in each run, which was used for x-ray photoemission spectroscopy analysis. In addition, a 10 nm Al_2O_3 layer was grown under the same conditions, with consistent electrical properties vs the 4 nm layers.

The surface topography was studied with atomic force microscopy (AFM, Asylum MFP-3D Infinity) in tapping mode. A transmission electron microscope (TEM) cross section sample was prepared from a 10 nm Al_2O_3 sample using a dual-beam focused ion beam (FIB, Helios Nano-Lab G3 FEI) microscope, and imaging was performed using a high-angle annular dark-field (HAADF) detector in scanning TEM (STEM) mode (FEI Titan 80–300 kV FEG-S/TEM). Magneto-transport measurements were performed in the van der Pauw geometry by depositing Au/Ti (100/5 nm) contacts (e-beam evaporation) after gently scratching the wafer corners with a scriber to ensure contact with all the layers. These contacts were bonded with Au wires. Hall and magnetoresistance (MR) measurements were performed using Physical Property Measurement System (PPMS, Quantum Design DynaCool) system in resistivity mode. The fixed measurement current was selected to be between 0.01 and 10 μA depending on sample conductivity. The Hall measurement includes high-field sweeps (−10 to 10 T) at 300 and 4 K (or the lowest measured temperature, depending on sample conductivity) and low-field sweeps (−1 to 1 T) every 30 K. The magnetoresistance measurements were also performed under high-field conditions, every 90 K until the lowest temperature, depending on the sample resistivity and the PPMS measurement limits.

X-ray photoelectron spectroscopy (XPS) measurements were carried out using a monochromated Al Kα (1486.6 eV) x-ray source and a Scienta Omicron EW4000 electron energy analyzer using 100 eV pass energy. The sample normal was aligned to the spectrometer axis to ensure a large information depth. Data were fit with the CasaXPS software after a Shirley background[34] subtraction.

III. RESULTS AND DISCUSSION

The surface topography of a 4 nm Al_2O_3 film grown on an STO substrate after 2 min of NH_3 plasma exposure exhibits long-range atomically flat terraces [Fig. 1(a)], indicating that the surface roughness is below the ~0.4 nm STO step height. The cross section STEM image [Fig. 1(b)] shows an abrupt interface between a 10 nm Al_2O_3 layer and the STO, for the most aggressive treatment—4 min of NH_3 plasma exposure, indicating that the NH_3 treatment does not result in significant structural changes in the STO surface. The slight crystalline contrast in the Al_2O_3 layer is ascribed to (unintentional) crystallization under the TEM beam.[28] The films are otherwise amorphous, within the sensitivity of x-ray diffraction (Fig. S1 and details therein), in agreement with our previous experience with comparable layers.[35,36]

The temperature dependence of the sheet resistance for six different NH_3 plasma durations, ranging from 30 s to 4 min, is presented in Fig. 2(a). Control samples without a plasma treatment were insulating beyond our measurement capability.[35] At room temperature, we observe a monotonous decrease in the sheet resistance as the plasma duration increases, ranging across three orders of magnitude. Previous studies of 2DEG systems with ALD Al_2O_3[26,37] and LAO/STO[4] reported typical sheet resistances in the range of 10^4–10^5 Ω/sq. A larger range and tunability were demonstrated via control of the growth oxygen environment[1,3] and via post-growth

06 December 2023 08:50:58

© Author(s) 2023

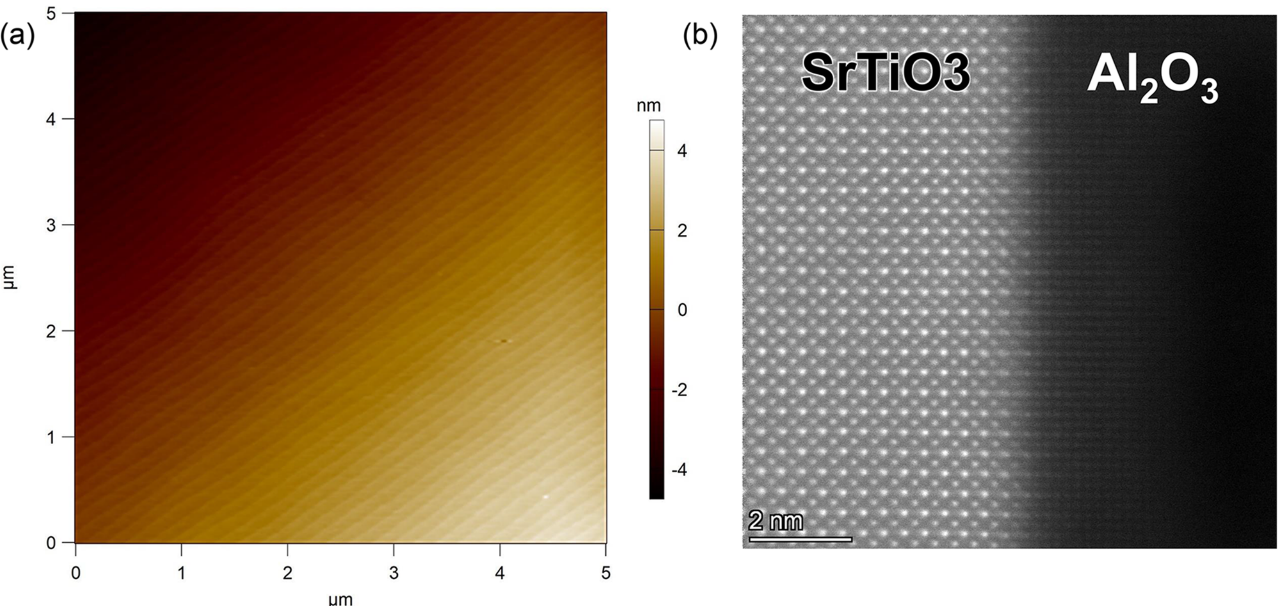

FIG. 1. Microstructural analysis of Al_2O_3–$SrTiO_3$ structures. (a) AFM image (5 × 5 μm^2) of a 4 nm Al_2O_3 layer on the (001) $SrTiO_3$ surface with 2 min of NH_3 plasma exposure. (b) Cross-sectional HAADF-STEM micrograph of a 10 nm Al_2O_3 layer with 4 min of NH_3 plasma exposure.

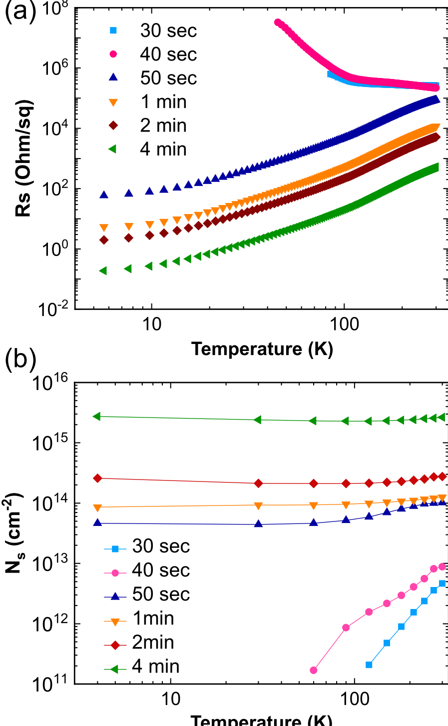

FIG. 2. Temperature dependence of (a) the sheet resistance and (b) the sheet carrier (N_s) density for varying NH_3 plasma durations (the lines are a guide to the eye). Samples with no plasma exposure exhibited resistivities beyond the measurement limit.

annealing at various oxygen pressures.[5] Recently, a two-order magnitude tunability at room temperature was demonstrated by doping[38] with a PLD process. Here, we report continuous tunability of the sheet resistance from 10^2 to 10^5 Ω/sq at room temperature. This large tunability demonstrates robust control of the interface conductivity using a simple pretreatment, which is part of a scalable deposition process. Modern ALD systems can process dozens of large wafers in a single run, providing a highly scalable and microelectronics-compatible route for oxide interfaces with tailor-made electronic properties. At low temperatures, this tunability range increases to at least six orders of magnitude [Fig. 2(a)].

The temperature-dependent sheet resistance further shows a metal–insulator transition (MIT) between 40 and 50 s of plasma pretreatment, as evident by the crossover from a negative (insulating) R_s–T slope until 40 s to a positive (metallic) slope from 50 seconds and above. Such a carrier density-dependent MIT is consistent with bulk $SrTiO_3$[39] and $SrTiO_3$-based 2DEG systems.[3,5,11,40,41]

Sheet carrier densities and mobility values were extracted by Hall measurements, from the transverse resistance vs the magnetic field behavior[42] (R_{xy}–B). Other than a single data point (4 min exposure, measured at 4 K, to be discussed later), all the R_{xy}–B data exhibited linear relations and were fitted accordingly as a single conductive channel.[43] The carrier density and mobility trends [Figs. 2(b) and S3] confirm the expectation that the conductivity tunability originates from the carrier density: the longer plasma exposure duration increases the degree of STO reduction, which is the source of the vacancy-induced electrons. Plasma durations longer than 4 min were not attempted in this work, but the effect of extended plasma is expected to saturate at some point, and it might result in the formation of different types of defects and even structural changes in the STO surface. The carrier density

06 December 2023 08:50:58

© Author(s) 2023

of the metallic regime is largely temperature-independent,[39,41,44] whereas the insulating region exhibits a thermally activated behavior.

The extracted mobility values exceed 10^4 cm^2 V^{-1} s^{-1} at low temperatures for the metallic samples (Fig. S3). These values are comparable to those for AlO_x/STO[43,45] and one order of magnitude lower than the highest reported values in the literature for γ-Al_2O_3/STO.[46,47] We ascribe the high mobility here to the chemical process of vacancy formation, which preserves the microstructural quality of the STO surface (Fig. 1). By contrast, in several reports, kinetic damage from the deposition (typically PLD) is the mechanism for vacancy formation, which can reduce the mobility. Therefore, the potential of the ALD technique to induce even higher mobilities is evident, all the while being scalable and suitable for mass production.

We consider the interpretation of the low-temperature Hall data and the possibility of multichannel conduction. This is done by looking for its fingerprint of nonlinear R_{xy}–B behavior.[20,48,49] After examining the low-temperature two-channel fits for all the conductive samples (Fig. S4 and discussion therein), such a behavior is found to be distinct only for the 4 min sample at 4 K. The origin of splitting into two types of carriers (chaneels) is due to selective orbital occupation; the Ti $3d_{xy}$ orbital is filled first and donates the first type of carriers. Once the $3d_{xy}$ is partially filled to a critical value, the higher-energy d_{xz} and d_{yz} orbitals begin to fill.[50] While anomalous Hall effect (AHE) is another possible source for a nonlinear R_{xy}–B behavior (due to possible Ti^{3+} magnetism), the absence of a Kondo resistivity upturn[51] in the R_S–T behavior [Fig. 2(a)] implies that AHE does not have a significant contribution here.

The two-channel Hall analysis (4 min, 4 K) yields two channels with a similar electron density of ~2.5 × 10^{15} cm^{-2} and dissimilar mobility values of 8 × 10^2 and 1.4 × 10^4 cm^2 V^{-1} s^{-1} [Fig. 2(c)]. Few studies have shown sheet carrier densities exceeding 10^{15} cm^{-2},[52–56] making the present result one of the highest reported to date. All previous reports of high carrier density systems were reported for epitaxial interfaces (mostly fabricated by PLD). Altogether, Fig. 2 exhibits one of the most tunable oxide interfaces ever reported, which can reach carrier densities that are comparable to the record reports; these interfaces are fabricated using a simple, scalable, highly tunable, and microelectronics-compatible material and process.

The results are consistent with the expected mechanism of reduction of the STO surface and creation of oxygen vacancies by the plasma treatment. The higher mobility in the present case is ascribed to the structural integrity of the topmost STO layers [Fig. 1(b)], owing to the low-energy nature of ALD vs the high kinetic energy of the more common PLD process. Moreover, the high mobility values suggest that it is a (quasi-) 2D system, and the 2DEG is centered in close proximity to the Al_2O_3/STO interface.[46]

The temperature-dependent carrier density behavior of the insulating samples (t = 30, 40 s) indicates that the carriers are thermally activated. This is confirmed by an Arrhenius plot (Fig. 3), where fits above 150 K exhibit a linear behavior with activation energies of ≈54 and 31 meV for 30 and 40 s plasma durations, respectively. We note that these values represent a range, with the exact slope value depending on the specific choice of temperature range

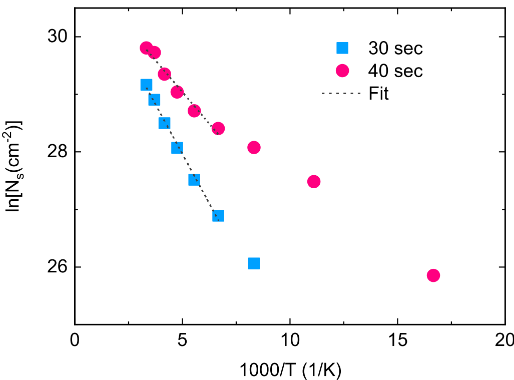

FIG. 3. Arrhenius plot of the sheet carrier density (N_s) vs the inverse temperature for the insulating samples of 30 and 40 s plasma exposure. The dashed lines represent the linear fits in the 300–150 K range.

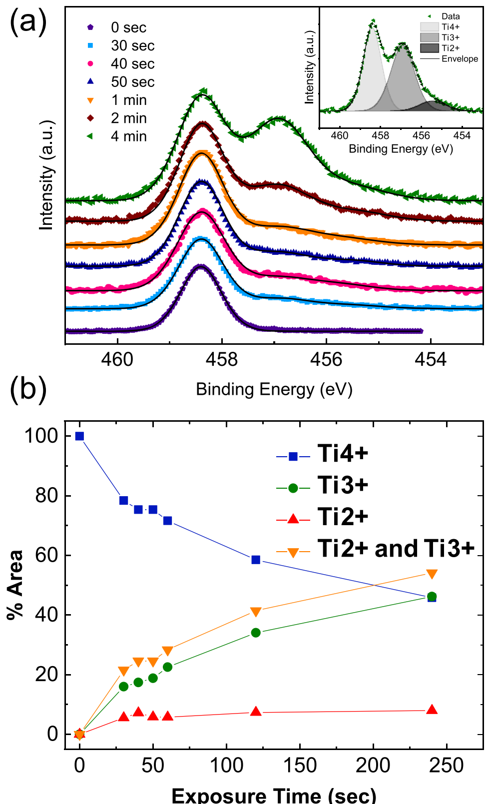

FIG. 4. (a) Ti $2p_{3/2}$ XPS spectra and fitting envelope of Al_2O_3–STO structure with different NH_3 plasma exposure durations. The spectra were obtained underneath a 4 nm Al_2O_3 layer. The inset is an example of a three-component (4+, 3+, and 2+) fit of the 4 min sample. (b) The relative area of the fit components and the sum of 3+ and 2+ areas obtained from the Ti $2p_{3/2}$ spectra vs the NH_3 plasma pretreatment duration (the lines are a guide to the eye).

06 December 2023 08:50:58

© Author(s) 2023

of the Arrhenius fit, where the deviation from linearity is ascribed to additional thermal processes. These values are in good agreement with previous reports of oxygen vacancy-induced donor levels of 30 meV for ALD–Al_2O_3/STO,[26] 25 meV for reduced STO,[57] and 18–189 meV for the related ALD–Al_2O_3/TiO_2 system[29] (the energy represents the depth of the donor below the conduction band). Altogether, Fig. 3 supports the NH_3 plasma-induced oxygen vacancy picture, with electron activation energy range in agreement with previous reports.

To gain further insights into the 2DEG formation mechanisms, XPS analysis of the buried Al_2O_3/STO interface was employed. The XPS spectra of Ti $2p_{3/2}$ consist of a major Ti^{4+} oxidation state (aligned to 458.4 eV) and a broad shoulder at lower binding energies (BEs), which is ascribed to Ti^{3+} and Ti^{2+} states[26,29,58–61] [Fig. 4(a)]. No constraints were applied to the fit in order to capture possible variations in the peak shapes; these were found to be negligible, and the peak offsets are in agreement with the literature[62] (see Table S2 for the full details). The relative area of the reduction-induced peaks (Ti^{3+} and Ti^{2+}) increases with the NH_3 pulse duration [Fig. 4(b)]. The absence of these features in the spectrum of the insulating sample without an NH_3 treatment confirms that the plasma treatment induces oxygen vacancies near the interface and that this is the mechanism behind the interfacial conductivity.[26,29] Furthermore, no nitrogen signal was observed in the N 1s spectral region (Fig. S5), which indicates that no nitrogen has been incorporated in the films, at least not in concentrations appreciable by XPS, which is below a percent level.[63]

IV. CONCLUSION

We synthesized Al_2O_3–STO interfaces using ALD and performed an NH_3 plasma pretreatment immediately before Al_2O_3 deposition. This procedure does not result in observable structural changes. The plasma duration was employed as a tuning parameter for the electronic properties of the conductive interface. Without plasma exposure, the interface is insulating, and between 30 s and 4 min of exposure leads to three orders of magnitude increase in conductivity (and six orders at 50 K). The origin of the conductivity increase is via an increase in the carrier density, without a significant effect on the mobility. We identify and explain this mechanism behind the conductivity tuning to be a reduction of the STO surface during pretreatment, a monotonous increase in suboxidized Ti features in XPS with increasing plasma exposure times. Altogether, our results highlight a scalable approach for synthesizing highly tunable oxide interfaces, driving oxide electronics closer toward mass-production capabilities and practical realization.

SUPPLEMENTARY MATERIAL

The supplementary material includes x-ray diffraction of an Al_2O_3 layer, room temperature electrical properties of the entire set of samples, discussion on the effect of light, data and discussion of the mobility, fiting and analysis of the two-channel mode magnetotransport and Hall data, XPS fitting parameters, and scans of the N 1s spectral region. A separate .xlsx file includes all the data used to prepare the figures of the paper and additional raw data.

ACKNOWLEDGMENTS

This work was funded by the Israel Science Foundation (ISF Grant No. 1351/21). F.T. acknowledges the support by research Grant No. 37338 (SANSIT) from Villum Fonden. Sample fabrication was performed with the support of the Technion's Micro-Nano Fabrication & Printing unit (MNF&PU), and characterization was performed with partial support from the Technion's Russell Berrie Nanotechnology Institute (RBNI). The authors thank Dr. Pini Shekhter (Tel Aviv University) for preliminary XPS measurements; Dr. Yaron Kauffmann, Dr. Galit Atia, and Dr. Larisa Popilevsky (Technion) for TEM imaging and sample preparation; and Tania Neverov, Dr. Anna Eyal, Valentina Korchnoy, Arkadi Gavrilov, and Tatiana Beker (Technion) for their valuable assistance with fabrication, processing, and measurements of the samples.

AUTHOR DECLARATIONS

Conflict of Interest

The authors have no conflicts to disclose.

Author Contributions

Dana Cohen-Azarzar: Data curation (lead); Formal analysis (equal); Methodology (equal); Writing – original draft (equal); Writing – review & editing (equal). **Maria Baskin**: Data curation (equal); Methodology (equal). **Andreas Lindblad**: Data curation (equal). **Felix Trier**: Conceptualization (equal); Formal analysis (equal); Methodology (equal). **Lior Kornblum**: Conceptualization (lead); Funding acquisition (lead); Methodology (equal); Supervision (lead); Writing – original draft (equal); Writing – review & editing (equal).

DATA AVAILABILITY

The data that support the findings of this study are available within the article and its supplementary material.

REFERENCES

[1] A. Ohtomo and H. Y. Hwang, Nature **427**, 423 (2004).
[2] N. Nakagawa, H. Y. Hwang, and D. A. Muller, Nat. Mater. **5**, 204 (2006).
[3] G. Herranz, M. Basletić, M. Bibes, C. Carrétéro, E. Tafra, E. Jacquet, K. Bouzehouane, C. Deranlot, A. Hamzić, J.-M. Broto, A. Barthélémy, and A. Fert, Phys. Rev. Lett. **98**, 216803 (2007).
[4] Z. Q. Liu, C. J. Li, W. M. Lü, X. H. Huang, Z. Huang, S. W. Zeng, X. P. Qiu, L. S. Huang, A. Annadi, J. S. Chen, J. M. D. Coey, T. Venkatesan, and Ariando, Phys. Rev. X **3**, 021010 (2013).
[5] C. Xu, C. Bäumer, R. A. Heinen, S. Hoffmann-Eifert, F. Gunkel, and R. Dittmann, Sci. Rep. **6**, 22410 (2016).
[6] C. Weiland, G. E. Sterbinsky, A. K. Rumaiz, C. S. Hellberg, J. C. Woicik, S. Zhu, and D. G. Schlom, Phys. Rev. B **91**, 165103 (2015).
[7] L. Qiao, T. C. Droubay, T. C. Kaspar, P. V. Sushko, and S. A. Chambers, Surf. Sci. **605**, 1381 (2011).
[8] F. Gunkel, C. Bell, H. Inoue, B. Kim, A. G. Swartz, T. A. Merz, Y. Hikita, S. Harashima, H. K. Sato, M. Minohara, S. Hoffmann-Eifert, R. Dittmann, and H. Y. Hwang, Phys. Rev. X **6**, 031035 (2016).
[9] L. Yu and A. Zunger, Nat. Commun. **5**, 5118 (2014).
[10] Y. Li, X. Wei, and J. Yu, J. Appl. Phys. **127**, 205302 (2020).
[11] P. Sharma, Z. Huang, M. Li, C. Li, S. Hu, H. Lee, J.-W. Lee, C.-B. Eom, S. J. Pennycook, J. Seidel, Ariando, and A. Gruverman, Adv. Funct. Mater. **28**, 1707159 (2018).
[12] B. Förg, C. Richter, and J. Mannhart, Appl. Phys. Lett. **100**, 053506 (2012).
[13] M. Hosoda, Y. Hikita, H. Y. Hwang, and C. Bell, Appl. Phys. Lett. **103**, 103507 (2013).

06 December 2023 08:50:58

© Author(s) 2023

[14]T. J. Seok, Y. Liu, H. J. Jung, S. B. Kim, D. H. Kim, S. M. Kim, J. H. Jang, D.-Y. Cho, S. W. Lee, and T. J. Park, ACS Nano **12**, 10403 (2018).
[15]L. Kornblum, Adv. Mater. Interfaces **6**, 1900480 (2019).
[16]N. Y. Chan, M. Zhao, J. Huang, K. Au, M. H. Wong, H. M. Yao, W. Lu, Y. Chen, C. W. Ong, H. L. W. Chan, and J. Dai, Adv. Mater. **26**, 5962 (2014).
[17]S. M. Kim, H. J. Kim, H. J. Jung, J.-Y. Park, T. J. Seok, Y.-H. Choa, T. J. Park, and S. W. Lee, Adv. Funct. Mater. **29**, 1807760 (2019).
[18]E. Lesne, Y. Fu, S. Oyarzun, J. C. Rojas-Sánchez, D. C. Vaz, H. Naganuma, G. Sicoli, J.-P. Attané, M. Jamet, E. Jacquet, J.-M. George, A. Barthélémy, H. Jaffrès, A. Fert, M. Bibes, and L. Vila, Nat. Mater. **15**, 1261 (2016).
[19]J. Varignon, L. Vila, A. Barthélémy, and M. Bibes, Nat. Phys. **14**, 322 (2018).
[20]L. M. Vicente-Arche, S. Mallik, M. Cosset-Cheneau, P. Noël, D. C. Vaz, F. Trier, T. A. Gosavi, C.-C. Lin, D. E. Nikonov, I. A. Young, A. Sander, A. Barthélémy, J.-P. Attané, L. Vila, and M. Bibes, Phys. Rev. Mater. **5**, 064005 (2021).
[21]S. Wu, X. Luo, S. Turner, H. Peng, W. Lin, J. Ding, A. David, B. Wang, G. Van Tendeloo, J. Wang, and T. Wu, Phys. Rev. X **3**, 041027 (2013).
[22]D. Miron, D. Cohen-Azarzar, B. Hoffer, M. Baskin, S. Kvatinsky, E. Yalon, and L. Kornblum, Appl. Phys. Lett. **116**, 223503 (2020).
[23]S. M. Kim, H. J. Kim, H. J. Jung, S. H. Kim, J.-Y. Park, T. J. Seok, T. J. Park, and S. W. Lee, ACS Appl. Mater. Interfaces **11**, 30028 (2019).
[24]K. Miller, F. Hartmann, B. Leikert, S. Kuhn, J. Gabel, M. Sing, R. Claessen, and S. Höfling, Appl. Phys. Lett. **118**, 153502 (2021).
[25]Y. Li, S. Kvatinsky, and L. Kornblum, Front. Phys. **9**, 642 (2021).
[26]S. W. Lee, Y. Liu, J. Heo, and R. G. Gordon, Nano Lett. **12**, 4775 (2012).
[27]T. Moon, H. J. Jung, Y. J. Kim, M. H. Park, H. J. Kim, K. D. Kim, Y. H. Lee, S. D. Hyun, H. W. Park, S. W. Lee, and C. S. Hwang, APL Mater. **5**, 042301 (2017).
[28]T. Moon, H. J. Lee, S. D. Hyun, B. S. Kim, H. H. Kim, and C. S. Hwang, Adv. Electron. Mater. **6**, 1901286 (2020).
[29]T. J. Seok, Y. Liu, J. H. Choi, H. J. Kim, D. H. Kim, S. M. Kim, J. H. Jang, D.-Y. Cho, S. W. Lee, and T. J. Park, Chem. Mater. **32**, 7662 (2020).
[30]V. Cremers, R. L. Puurunen, and J. Dendooven, Appl. Phys. Rev. **6**, 021302 (2019).
[31]S. M. George, Chem. Rev. **110**, 111 (2010).
[32]G. Koster, B. L. Kropman, G. J. H. M. Rijnders, D. H. A. Blank, and H. Rogalla, Appl. Phys. Lett. **73**, 2920 (1998).
[33]D. Miron, I. Krylov, M. Baskin, E. Yalon, and L. Kornblum, J. Appl. Phys. **126**, 185301 (2019).
[34]D. A. Shirley, Phys. Rev. B **5**, 4709 (1972).
[35]D. Cohen-Azarzar, M. Baskin, and L. Kornblum, J. Appl. Phys. **123**, 245307 (2018).
[36]Y. Li, W. Wang, D. Zhang, M. Baskin, A. Chen, S. Kvatinsky, E. Yalon, and L. Kornblum, Adv. Electron. Mater. **9**, 2200800 (2022).
[37]T. Q. Ngo, N. J. Goble, A. Posadas, K. J. Kormondy, S. Lu, M. D. McDaniel, J. Jordan-Sweet, D. J. Smith, X. P. A. Gao, A. A. Demkov, and J. G. Ekerdt, J. Appl. Phys. **118**, 115303 (2015).
[38]Y. Gan, Y. Zhang, S. Jiang, H. Zhang, X. Guan, L. Yan, F. Hu, R. Yu, J. Sun, H. Ding, K. Yang, Y. Chen, and B. Shen, Appl. Phys. Lett. **121**, 111601 (2022).
[39]A. Spinelli, M. A. Torija, C. Liu, C. Jan, and C. Leighton, Phys. Rev. B **81**, 155110 (2010).
[40]T. A. Cain, P. Moetakef, C. A. Jackson, and S. Stemmer, Appl. Phys. Lett. **101**, 111604 (2012).
[41]P. Moetakef, T. A. Cain, D. G. Ouellette, J. Y. Zhang, D. O. Klenov, A. Janotti, C. G. Van de Walle, S. Rajan, S. J. Allen, and S. Stemmer, Appl. Phys. Lett. **99**, 232116 (2011).
[42]L. Kornblum, E. N. Jin, O. Shoron, M. Boucherit, S. Rajan, C. H. Ahn, and F. J. Walker, J. Appl. Phys. **118**, 105301 (2015).
[43]B. Leikert, J. Gabel, M. Schmitt, M. Stübinger, P. Scheiderer, L. Veyrat, T. L. Lee, M. Sing, and R. Claessen, Phys. Rev. Mater. **5**, 065003 (2021).
[44]L. Kornblum, J. Faucher, M. D. Morales-Acosta, M. L. Lee, C. H. Ahn, and F. J. Walker, J. Appl. Phys. **123**, 025302 (2018).
[45]K. Gao, X. R. Ma, Q. L. Li, X. H. Zhang, J. P. Xu, Y. Sun, and G. Yu, Europhys. Lett. **138**, 66003 (2022).
[46]Y. Z. Chen, N. Bovet, F. Trier, D. V. Christensen, F. M. Qu, N. H. Andersen, T. Kasama, W. Zhang, R. Giraud, J. Dufouleur, T. S. Jespersen, J. R. Sun, A. Smith, J. Nygård, L. Lu, B. Büchner, B. G. Shen, S. Linderoth, and N. Pryds, Nat. Commun. **4**, 1371 (2013).
[47]P. Schütz, D. V. Christensen, V. Borisov, F. Pfaff, P. Scheiderer, L. Dudy, M. Zapf, J. Gabel, Y. Z. Chen, N. Pryds, V. A. Rogalev, V. N. Strocov, C. Schlueter, T.-L. Lee, H. O. Jeschke, R. Valentí, M. Sing, and R. Claessen, Phys. Rev. B **96**, 161409 (2017).
[48]F. Gunkel, S. Hoffmann-Eifert, R. A. Heinen, D. V. Christensen, Y. Z. Chen, N. Pryds, R. Waser, and R. Dittmann, ACS Appl. Mater. Interfaces **9**, 1086 (2017).
[49]F. Gunkel, C. Lenser, C. Baeumer, F. Borgatti, F. Offi, G. Panaccione, and R. Dittmann, APL Mater. **6**, 076104 (2018).
[50]P. Delugas, A. Filippetti, V. Fiorentini, D. I. Bilc, D. Fontaine, and P. Ghosez, Phys. Rev. Lett. **106**, 166807 (2011).
[51]Y. Hong, M.-A. Rose, Z. Zhang, M. Li, L. Heymann, S. He, and F. Gunkel, Phys. Rev. Appl. **18**, 034012 (2022).
[52]F. Trier, D. V. Christensen, and N. Pryds, J. Phys. D: Appl. Phys. **51**, 293002 (2018).
[53]P. Xu, T. C. Droubay, J. S. Jeong, K. A. Mkhoyan, P. V. Sushko, S. A. Chambers, and B. Jalan, Adv. Mater. Interfaces **3**, 1500432 (2016).
[54]E. N. Jin, L. Kornblum, D. P. Kumah, K. Zou, C. C. Broadbridge, J. H. Ngai, C. H. Ahn, and F. J. Walker, APL Mater. **2**, 116109 (2014).
[55]D. V. Christensen, Y. Frenkel, P. Schütz, F. Trier, S. Wissberg, R. Claessen, B. Kalisky, A. Smith, Y. Z. Chen, and N. Pryds, Phys. Rev. Appl. **9**, 054004 (2018).
[56]Y. Kozuka, M. Kim, H. Ohta, Y. Hikita, C. Bell, and H. Y. Hwang, Appl. Phys. Lett. **97**, 222115 (2010).
[57]Z. Q. Liu, D. P. Leusink, X. Wang, W. M. Lü, K. Gopinadhan, A. Annadi, Y. L. Zhao, X. H. Huang, S. W. Zeng, Z. Huang, A. Srivastava, S. Dhar, T. Venkatesan, and Ariando, Phys. Rev. Lett. **107**, 146802 (2011).
[58]P. Schütz, F. Pfaff, P. Scheiderer, Y. Z. Chen, N. Pryds, M. Gorgoi, M. Sing, and R. Claessen, Phys. Rev. B **91**, 165118 (2015).
[59]A. B. Posadas, K. J. Kormondy, W. Guo, P. Ponath, J. Geler-Kremer, T. Hadamek, and A. A. Demkov, J. Appl. Phys. **121**, 105302 (2017).
[60]Y. Chen, N. Pryds, J. E. Kleibeuker, G. Koster, J. Sun, E. Stamate, B. Shen, G. Rijnders, and S. Linderoth, Nano Lett. **11**, 3774 (2011).
[61]M. S. J. Marshall, D. T. Newell, D. J. Payne, R. G. Egdell, and M. R. Castell, Phys. Rev. B **83**, 035410 (2011).
[62]B. Psiuk, J. Szade, M. Pilch, and K. Szot, Vacuum **83**, S69 (2009).
[63]S. Oswald, *Encyclopedia of Analytical Chemistry* (John Wiley & Sons, Ltd., 2006).

06 December 2023 08:50:58

© Author(s) 2023